



MID-AMERICA TRANSPORTATION CENTER

Report # MATC-UI: 145-5

Final Report
WBS: 25-1121-0005-145-5

UNIVERSITY OF
Nebraska
Lincoln

THE UNIVERSITY
OF IOWA

THE UNIVERSITY OF
KU
KANSAS

MISSOURI
S&T

LINCOLN
UNIVERSITY
MISSOURI



UNIVERSITY OF
Nebraska
Omaha

University of Nebraska
Medical Center

KU MEDICAL
CENTER
The University of Kansas

Real-Time Flood Forecasting for River Crossings - Phase V

Witold Krajewski, PhD

Rose & Joseph Summers Chair in Water Resources Engineering
Faculty Research Engineer, IIHR - Hydroscience & Engineering
Director, Iowa Flood Center
The University of Iowa

Nicolás Velásquez, PhD

Assistant Researcher, Iowa Flood Center
Department of Civil and Environmental Engineering
The University of Iowa

THE UNIVERSITY
OF IOWA

2023

A Cooperative Research Project sponsored by
U.S. Department of Transportation- Office of the Assistant
Secretary for Research and Technology

MATC

The contents of this report reflect the views of the authors, who are responsible for the facts and the accuracy of the information presented herein. This document is disseminated in the interest of information exchange. The report is funded, partially or entirely, by a grant from the U.S. Department of Transportation's University Transportation Centers Program. However, the U.S. Government assumes no liability for the contents or use thereof.

Real-Time Flood Forecasting for River Crossings – Phase V

Witold Krajewski, PhD, P.I.
Rose & Joseph Summers Chair in Water
Resources Engineering
Faculty Research Engineer, IIHR -
Hydroscience & Engineering
Director, Iowa Flood Center
The University of Iowa

Nicolás Velásquez, PhD, P.I.
Assistant Researcher, Iowa Flood Center
Department of Civil and Environmental
Engineering
The University of Iowa

A Report on Research Sponsored by

Mid-America Transportation Center

University of Nebraska–Lincoln

May 2023

Technical Report Documentation Page

1. Report No. 25-1121-0005-145-5	2. Government Accession No.	3. Recipient's Catalog No.	
4. Title and Subtitle Real-Time Flood Forecasting for River Crossings – Phase V		5. Report Date May 2023	
		6. Performing Organization Code	
7. Author(s) Witold Krajewski, PhD ORCID: 0000-0002-3477-9281 Nicolas Velasquez, PhD ORCID: 0000-0001-8207-5492		8. Performing Organization Report No. 25-1121-0005-145-5	
9. Performing Organization Name and Address Mid-America Transportation Center Prem S. Paul Research Center at Whittier School 2200 Vine St. Lincoln, NE 68583-0851		10. Work Unit No. (TRAIS)	
		11. Contract or Grant No. 69A3551747107	
12. Sponsoring Agency Name and Address Office of the Assistant Secretary for Research and Technology 1200 New Jersey Ave., SE Washington, D.C. 20590		13. Type of Report and Period Covered Final Report, September 2020 – December 2021	
		14. Sponsoring Agency Code MATC TRB RiP No. 91994-100	
15. Supplementary Notes			
16. Abstract We have developed a generic prototype of a flood-forecasting model that is transferable to other locations around the Midwest to provide monitoring and forecasting of flood potential at critical infrastructure points, such as bridges, where streamflow gauges are not available. A real-time web-based visualization platform to display the model predictions has been implemented. The platform will display the river network upstream from the point of interest and a time control slider that will allow exploring the evolution of flows everywhere in the network over the past several days, and about a week into the future. The model uses in-house developed radar-rainfall maps updated every 5 minutes with the spatial resolution of about 0.5 km currently covering the Iowa domain and extending some 100 km into the neighboring states. For the future rainfall, we use predictions for the National Weather Service High-Resolution Rapid Refresh (HRRR) forecasting system. The system provides hourly accumulation products for up to 20 hours ahead. Our system expands the forecasting capabilities of the current NWS by providing predictions at locations that have not been historically gauged.			
17. Distribution Statement			
18. Security Classif. (of this report) Unclassified	19. Security Classif. (of this page) Unclassified	20. No. of Pages 36	21. Price

Table of Contents

Disclaimer	vii
Abstract	viii
Chapter 1 Preliminaries: The Iowa Flood Center HLM hydrological model	1
Chapter 2 HLM model improvements	5
2.1 High-definition network.....	5
2.2 Snow process representation.....	8
2.3 Implementation of the TETIS model in HLM	16
2.4 Rainfall products evaluation	19
2.5 Upstream data assimilation	20
Chapter 3 Performance evaluation tool.....	23
Chapter 4 Technology transfer.....	27
4.1 HLM implementation.....	27
4.2 Bridge sensors installation	30
Chapter 5 Conclusions	34

List of Figures

Figure 1.1 (a) illustration of landscape decomposition into hillslopes and decomposition of the river network into channel link and (b) vertical soil profile and control volumes included in the hydrological model.	1
Figure 2.1 Example of the new HLM network following NHDplus closely.....	6
Figure 2.2 Processed regions using the NHDplus network and DEM.....	7
Figure 2.3 Example of the new HLM network following NHDplus closely.....	8
Figure 2.4 Representation of the hillslope processes in HLM. a) HLM-NoSnow, b) HLM-FSnow, and c) HLM-PSnow model scheme. Blue arrows represent precipitation P and $qsnow$. Yellow arrows represent evapotranspiration from Sp , St , and Ss . Green arrows represent linear fluxes between storages. Purple arrows represent nonlinear fluxes.	10
Figure 2.5 HLM flow simulations (color lines) and USGS gauges flow observations (black dots) during the flood of March 2019. Blue lines correspond to HLM-no-snow, yellow to HLM-F-snow, and red to HLM-Snow.	11
Figure 2.6 Mean SWE accumulation (in cm) during the March 2019 flood event. a) HLM (blue line) and NSIDC (dots) mean SWE over the Nishnabotna watershed. b) NSIDC SWE estimations for March 6, 9, 11, and 13. c) HLM-FSnow SWE estimations for March 6, 9, 11, and 13.....	13
Figure 2.7 Mean KGE computed at the USGS gauges in Iowa using HLM-Snow. a) Long-term KGE comparing the observed records between 2002 and 2020. b) Mean KGE comparing only the results between December and April. c) March 2019 KGE.	14
Figure 2.8 March 2019 event ΔQp and KGE performance in function of its observed magnitude or peak ratio ($q(\max, 2019)/q_{max}$). a) peak ratio vs ΔQp , b) ΔQp estimated at each gauge, c) peak ratio vs. the KGE, and d) ΔQp frequency.	15
Figure 2.9 Schematic of the TETIS model structure in HLM.	16
Figure 2.10 Difference between the TETIS KGE and Toplayer KGE. Positive values (red) represent regions where TETIS outperformed the Toplayer. Negative values (green) represent the opposite.	17
Figure 2.11 Flow simulations obtained at basins of the Des Moines Lobe landform (left column) and basins in Western Iowa.	18
Figure 2.12 HLM KGE performance using IFC-RA (a) and IFC-RZ (b). The dots correspond to the USGS gauges in Iowa. c) presents the frequency distribution of both setups.	19
Figure 2.13 HLM volumetric bias using IFC-RA (a) and IFC-RZ (b) and MRMS (c). The dots correspond to the USGS gauges in Iowa. d) presents the frequency distribution of the three setups.....	20
Figure 2.14 EKI Routing parameters estimation and simulated streamflow.	21
Figure 2.15 Results from the EKI data assimilation performed at Shell Rock River (4,487 km ²) upstream of Cedar River (16,861 km ²). The blue area represents the 10-90 interquartile region obtained by the particles, and the blue line is the particles' mean. The dashed black line represents the observed discharge, and the green line is the reference provided by HLM using MRMS without data assimilation.....	22
Figure 3.1 Top panels of the hydrologic modeling validation tool.....	23
Figure 3.2 Streamflow plot panel showing the results for Clear Creek, Iowa.....	24
Figure 3.3 Streamflow plot panel showing the Clear Creek, Iowa results, in log-scale.	25

Figure 3.4 Event-based analysis using the platform.	26
Figure 4.1 Mean Observed (orange) and simulated (blue) SWE over the Elkhorn watershed.....	28
Figure 4.2 HLM-Snow simulations at the Elkhorn River Watershed for March 2019.....	29
Figure 4.3 Elkhorn River web platform example.	30
Figure 4.4 Elkhorn River Network (blue lines), USGS gauges (green), and installed bridge sensors (red). Image taken from Koya et al. (2023).....	31
Figure 4.5 Synthetic rating curves developed for each installed level gauge. Taken from Koya et al. (2023).	32

List of Abbreviations (optional)

Mid-America Transportation Center (MATC)

Nebraska Transportation Center (NTC)

Iowa Flood Center (IFC)

Hillslope Link Model (HLM)

Disclaimer

The contents of this report reflect the views of the authors, who are responsible for the facts and the accuracy of the information presented herein. This document is disseminated in the interest of information exchange. The report is funded, partially or entirely, by a grant from the U.S. Department of Transportation's University Transportation Centers Program. However, the U.S. Government assumes no liability for the contents or use thereof.

Abstract

In this research, we have developed a generic prototype of a flood-forecasting model that is transferable to other locations around the Midwest to monitor and forecast flood potential at critical infrastructure points, such as bridges, where streamflow gauges are unavailable. Our efforts have centered on improving runoff generation representation and transferring our tools to the University of Nebraska. In this phase, we focus on improving the model and transferring our technology. As part of our improvements, we included snow processes in a hillslope link model (HLM), added a different runoff generation scheme, and developed a data assimilation approach to improve forecasts using downstream observations. Additionally, we describe the outcomes of our technology transfer to the University of Nebraska implementing HLM-Snow in the Elkhorn River watershed.

Chapter 1 Preliminaries: The Iowa Flood Center HLM hydrological model

The Iowa Flood Center hydrological model, Hillslope-Link Model (HLM), is a distributed hillslope-scale rainfall-runoff model that partitions Iowa into over three million individual control volumes following the landscape decomposition outlined in Mantilla and Gupta (2005). The model is parsimonious, using ordinary differential equations to describe transport between adjacent control volumes. This characteristic reduces the computational resources needed by capturing the most essential features of the rainfall runoff transformation; it uses only a few parameters to obtain acceptable results. The model partitions the river network into river links (the portion of a river channel between two junctions of a river network) and the landscape into hillslopes (adjacent areas that drain into the links).

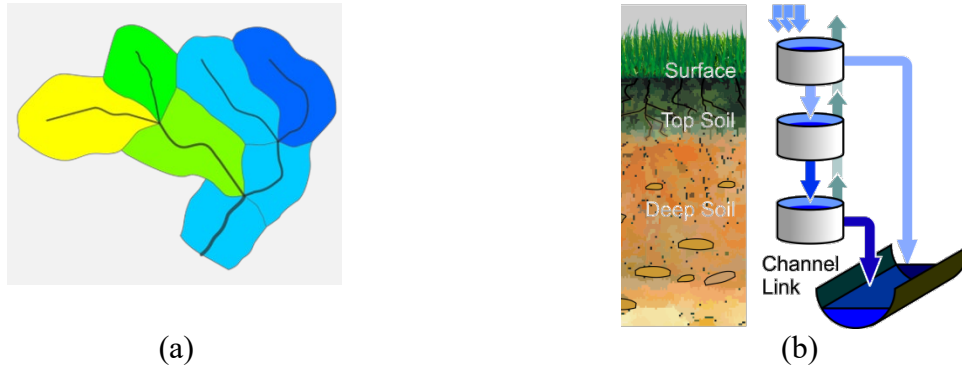


Figure 1.1 (a) illustration of landscape decomposition into hillslopes and decomposition of the river network into channel link and (b) vertical soil profile and control volumes included in the hydrological model.

Mass conservation equations form the system of coupled nonlinear ordinary differential equations that represent changes in the water storage in the hillslope surface (s_{surf}), top soil (s_{tops}), and deep soil (s_{deeps}) given by,

$$\left\{ \begin{array}{l} \frac{ds_{surf}(t)}{dt} = p(t) - q_{runoff}(t) - q_{infil}(t) - e_{surf}(t) \end{array} \right. \quad (1.1)$$

$$\left\{ \begin{array}{l} \frac{ds_{tops}(t)}{dt} = q_{infil}(t) - q_{percol}(t) - e_{tops}(t) \end{array} \right. \quad (1.2)$$

$$\left\{ \begin{array}{l} \frac{ds_{deeps}(t)}{dt} = q_{percol}(t) - q_{baseflow}(t) - e_{deeps}(t) \end{array} \right. \quad (1.3)$$

Fluxes in, across, and out of the vertical hillslope control volumes include precipitation $p(t)$, overland runoff $q_{runoff}(t)$, infiltration into the topsoil q_{infil} , percolation from the topsoil into the deeper soils $q_{percol}(t)$, baseflow into the channel $q_{baseflow}(t)$, and evaporation from the ponded, topsoil, and deep soil layers ($e_{surf}(t)$, $e_{tops}(t)$ and $e_{deeps}(t)$, respectively). The model assumes that percolation flux is a linear function of the amount of water stored at time t in the topsoil $q_{percol} = k_{percol} \cdot S_{tops}$ and that the baseflow is a linear function of the water stored in deep soil $q_{baseflow} = k_{baseflow} \cdot S_{deeps}$. Overland runoff is a power function of the water stored on the hillslope surface (consistent with Manning's equation) given by,

$$q_{runoff} = k_{runoff} S_{surf}^{1.67} \quad (1.4)$$

and infiltration is a nonlinear function of soil moisture content (S_{tops}/T_{tops}), where T_{tops} is the thickness of the topsoil layer (i.e., A-horizon) and a linear function of hydraulic head s_{surf} given by,

$$q_{infil} = k_{dry} \left(1 - \frac{S_{tops}}{T_{tops}} \right)^\phi s_{surf} \quad (1.5)$$

Where k_{dry} corresponds to the case of dry soil and, similarly to k_{runoff} , k_{percol} , and $k_{baseflow}$, can be interpreted as a time constant (residence time) of the respective storage component. The average hillslope area (a_h) for the elements in the distributed model is 0.05 km², and average link length (l_{link}) is 400 m. Note that $a_h/(2l_{link})$ is the hillslope length. The exponent φ is a nonlinearity introduced by the change in the potential matrix of the soil column as soil moisture changes with time.

The HLM should be thought of as a modeling system rather than a single specific model. As the equations describing hillslope-scale processes are separated from the numerical solver, it is rather easy to explore different mathematical descriptions for water fluxes. For example, one can consider simplifications such as a constant runoff coefficient or water transport velocity, or one can formulate these components based on the available physical characteristics.

Water transport through the river network is nonlinear and governs how channel links propagate flow through the river network. Formulated in the context of a mass conservation equation developed by Gupta and Waymire (1998), it uses the water velocity parameterization given by Mantilla (2007) as,

$$\frac{dq_{link}(t)}{dt} = \frac{v_0 q_{link}^{\lambda_1}(t) A^{\lambda_2}}{(1 - \lambda_1) l} \left[a_h \left(k_{runoff} S_{surf}^{1.67}(t) + k_{baseflow} S_{deeps}(t) \right) - q_{link}(t) + q_1(t) + q_2(t) \right] \quad (1.6)$$

where q_{link} is the discharge from the link at time t , a_h is the total hillslope area draining to the link, $q_1(t)$ and $q_2(t)$ are the incoming flows of the upstream tributaries, A is the upstream basin area, and λ_1 , λ_2 , and v_0 are global parameters of the water velocity component of the model and are set to 0.2, -0.1, and 0.3, respectively. The model can capture the main features of the hydrographs including the maximum stage. We used the model in several studies e.g. Ayalew et

al. (2014) and Cunha et al. (2012). We also discuss the model performance in Krajewski et al. (2017). The model is driven by radar-rainfall estimated from Level II NEXRAD data from seven WSR-88D weather radars covering the state of Iowa. The maps of rainfall intensity have spatial resolution of about 0.25 km^2 and are updated every five minutes. The algorithms are described in Krajewski et al. (2013) and Seo and Krajewski (2015).

An important aspect of our modeling approach is the avoidance of calibration. Instead, we rely on detailed information of the physical properties we model. This includes the topography, land use and land cover, soil properties, and details of the main forcing, i.e., precipitation. Comparing simulation results to streamflow observations across Iowa validates the model formulation and parameterization. Therefore, we can view the model as data-intensive and calibration-free when used in forecast-mode. This, in turn, implies that with more detailed, relevant, and accurate data, including model states and physical domain characterization as well as the driving inputs, the model will work better. The model is fully automatic in the sense that no corrections are applied to the model as it moves forward in time once initial and boundary conditions are imposed.

The model predicts the streamflow fluctuations associated with storm events over the catchment of interest using current observations of rainfall, and rainfall forecasts. The effect of storms on river ways is usually delayed ranging from days to weeks. Each point of interest in the landscape (bridge, culvert) can then be categorized according to the maximum warning time. The web interface provides a visual tool to show when a particular location will be impacted, and it provides an inundation map for the particular peak flow expected for that location. Inundation maps are more effective tools in communicating the effects of flooding than crest stages at specific locations.

Chapter 2 HLM model improvements

This chapter delves into the process of advancing HLM. We explore the integration of a high-definition network, the representation of snow processes, the evaluation of two IFC rainfall products, and the assimilation of data upstream. These critical components play a pivotal role in enhancing the accuracy and reliability of hydrological forecasts. We aim to refine our understanding of water resources and improve our forecasting capabilities.

2.1 High-definition network

We have been working on a methodology to develop a network for HLM that closely follows the observed network and is informed of the rivers' and creeks' names. Our development uses Digital Elevation Models (DEM) with a resolution of 10m and the official streamflow network of the U.S. (NHDplusV2) created by the USGS. We start by converting the NHDplus network into a raster format using the properties of the DEM. Then, we burn the NHDplus raster into the DEM. Finally, we process the burned DEM using TauDEM. We obtain a network suited for HLM closely following NHDplus from the process (Figure 2.1).

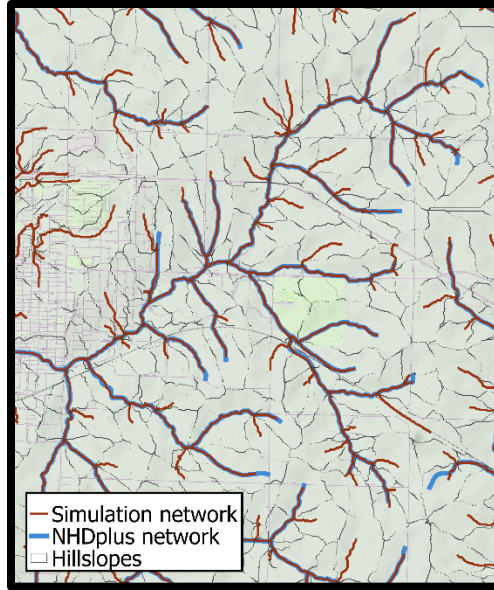


Figure 2.1 Example of the new HLM network following NHDplus closely.

Depending on the size of the area processed, the described process may be computationally intensive. In our case, we processed Iowa in four regions using the definitions of level four HUCs (see Figure 2.2), and the four regions in the University of Iowa HPC. The process for each domain took around one day. Nevertheless, the process only needs to be done once for each region.

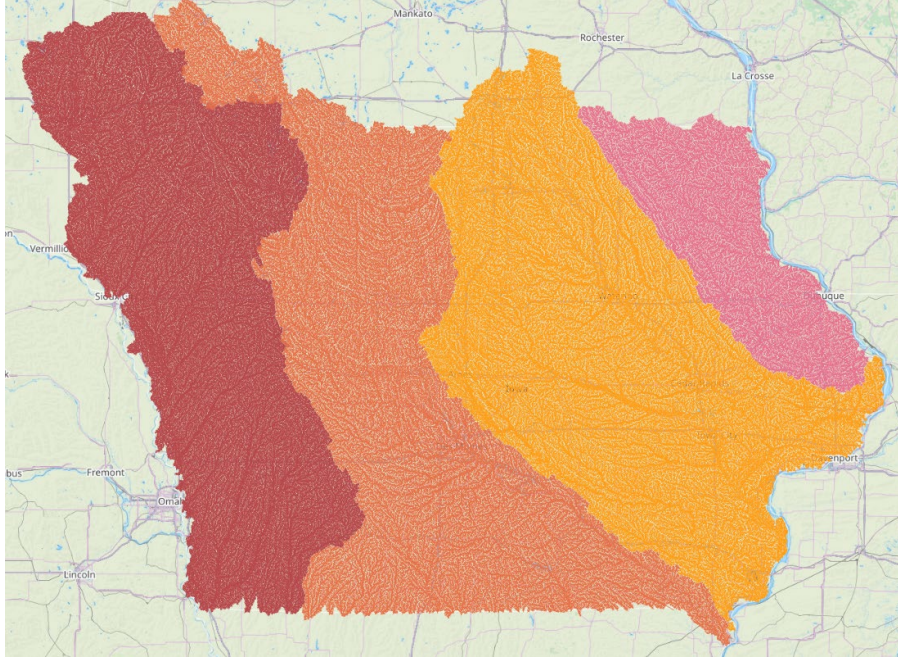


Figure 2.2 Processed regions using the NHDplus network and DEM.

Additionally, we developed an algorithm to perform a conflation between the HLM and NHDplusV2 networks. The detailed description of the network allowed us to perform hydrological simulations at a scale that corresponds with the observed features of the landscape. In the process, we assign NHDplus IDS to each HLM network element (see Figure 2.3). The conflation connects HLM and NHDplusV2 segments allowing us to perform future comparisons with the National Water Model (NWM). Also, we established a link between the HLM segments and the names of the rivers allowing more interaction in the communication of the forecasts. The described connection represents a significant improvement that allows performing regional flood forecasts on a human scale.

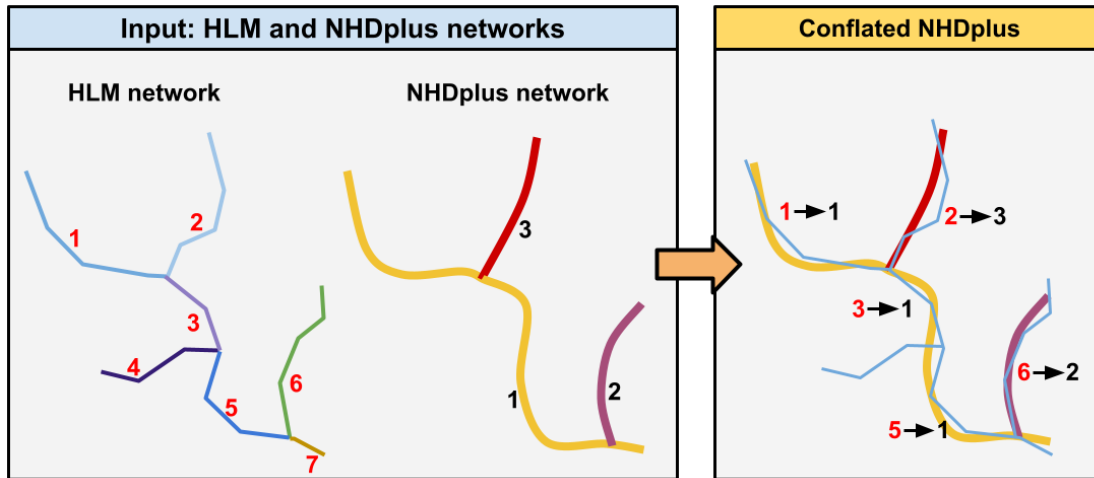


Figure 2.3 Example of the new HLM network following NHDplus closely.

Currently, we are using the conflated network in some regions of Iowa. The described approach represents a significant step in developing a flood forecasting system. Following the observed streamflow network allows increased model performance and more accurate forecasts. Moreover, it also allows better communication with the authorities and communities. On the other hand, the conflation represents a significant advance that allows performing regional flood forecasts on a human scale and the eventual use of automated systems.

The methodology described here can be easily extended to other areas of the contiguous U.S. since it only uses NHDplus, a product available in the country. In our case, we limit the regions using level four HUCs. We decided to use this limitation to reduce the number of elements simulated in HLM. With our approach, each region has around 200K elements, which allows us to explore HLM results without having long execution times.

2.2 Snow process representation

We developed a snow parameterization for HLM (HLM-Snow) in conjunction with the University of Nebraska. Following the formulation proposed by Koya et al. (2023), we

implemented HLM-Snow to represent snow accumulation and melting processes on hillslopes. HLM-Snow adds a storage S_{snow} and uses the temperature threshold (TT) method to represent Snow Water Equivalent (SWE) accumulation and melting. Compared to other TI schemes, TT is among the simplest (Kienzle, 2008), adding just two parameters to the model and keeping its parsimony. In TT, depending on a threshold temperature, T_b precipitation falls as liquid rainfall or SWE. If the air temperature $T(t)$ is lower than T_b , precipitation accumulates in the snow storage S_{snow} as SWE. When $T(t)$ is above T_b , snowmelt takes place at S_{snow} with a rate of D . The given description can be expressed as follows:

$$q_{snow} = \begin{cases} P & , \quad T < T_b \\ 0 & , \quad T \geq T_b \end{cases} \quad (2.1)$$

In equation (2.1), q_{snow} represents the rainfall P becoming SWE (S_{snow}). In the threshold scheme, P is equal to zero when $T < T_b$. Moreover, snowmelt, $q_{melt,p}$ subtracts water from S_{SWE} when $T \geq T_b$, the equation is as follows:

$$q_{melt,p} = \min(D \cdot T, S_{SWE}) \quad (2.2)$$

After $q_{melt,p}$ is computed, S_{SWE} is updated as follows:

$$\frac{dS_{SWE}}{dt} = q_{snow} - q_{melt,p} \quad (2.3)$$

The melted water from S_{SWE} updates the ponded storage (S_p), modifying equation (1.1)

as follows:

$$\frac{dS_p}{dt} = P - q_{pL} - q_{pT} + q_{melt,p} - e_p \quad (2.4)$$

Additionally, when $T < T_b$ we assume zero flow from the ponded storage to the topsoil ($q_{pT} = 0$), representing the ground being frozen.

We tested the model in the Nishnabotna River in Iowa, by comparing it against the original HLM (HLM-NoSnow) and the HLM using snowmelt as an additional force (HLM-Fsnow). Figure 2.4 presents the three configurations that we implemented in the test.

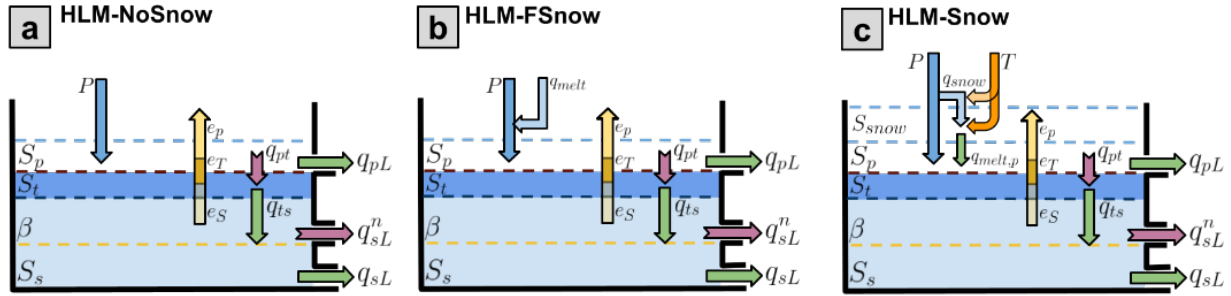


Figure 2.4 Representation of the hillslope processes in HLM. a) HLM-NoSnow, b) HLM-FSnow, and c) HLM-PSnow model scheme. Blue arrows represent precipitation P and q_{snow} . Yellow arrows represent evapotranspiration from S_p , S_t , and S_s . Green arrows represent linear fluxes between storages. Purple arrows represent nonlinear fluxes.

Figure 2.5 shows the simulated and observed flows at the five USGS gauges. According to the hydrograph plots, HLM-NoSnow underestimates the total volume and peak flows, evidencing the snow processes' relevance. In contrast, HLM-FSnow overestimates both variables in the five gauges. On the other hand, HLM-Snow accurately represents them. Besides,

compared with HLM-FSnow, HLM-Snow matches the observations simulating one peak instead of two.

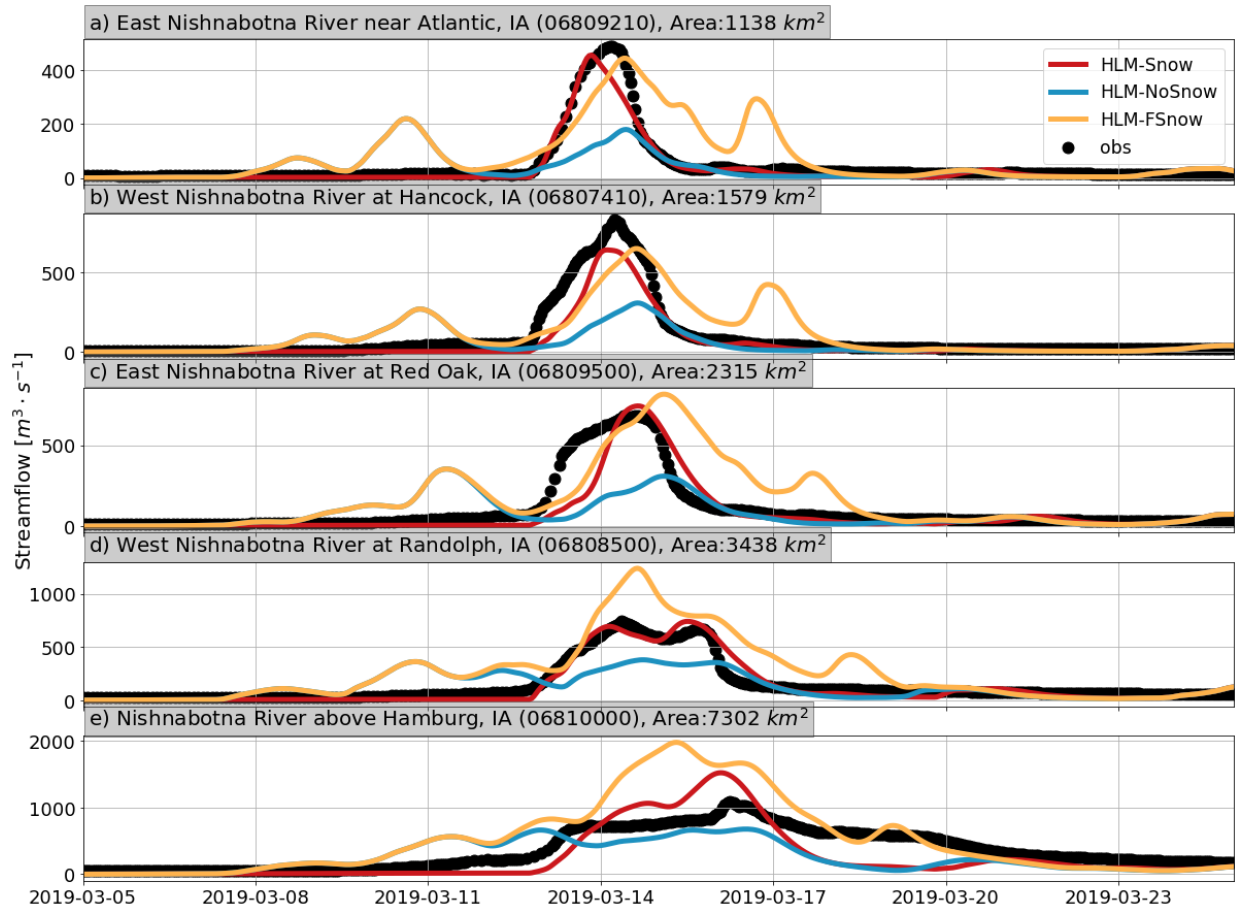


Figure 2.5 HLM flow simulations (color lines) and USGS gauges flow observations (black dots) during the flood of March 2019. Blue lines correspond to HLM-no-snow, yellow to HLM-F-snow, and red to HLM-Snow.

In addition to the discharge comparison, we compared the daily NSIDC SWE observations between March 3 and March 16, 2019. In this period, HLM-Snow accurately estimated the SWE oscillations (Figure 2.6a). This accuracy is evidenced by a KGE of 0.93, an NSE of 0.87, and a volumetric difference of -1.25%. In addition to the temporal comparisons, we present spatial differences between both SWE products at four dates (Figure 2.6b and c). Dates 1

and 2 compare the initial SWE storage and its initial accumulation. Date 3 compares SWE values after the precipitation event of March 9 (see Figure 2.6b) and Date 4, SWE during the flood event around March 13. In the four dates, HLM-Snow provides a spatial distribution that follows NSIDC. However, there are some differences. Between Dates 2 and 4, NSIDC-SWE exhibits more significant accumulations in the West and North, while HLM-SWE accumulations also include the East. We also noticed that NSIDC-SWE fields are more heterogeneous than HLM-SWE ones. We attribute most of these differences to rainfall uncertainties, the TI method's simplicity, and the use of temperature derived from one weather gauge. Regardless of the reason, the overall performance of HLM-Snow indicates that capturing the SWE total is more relevant than capturing its spatial distribution.

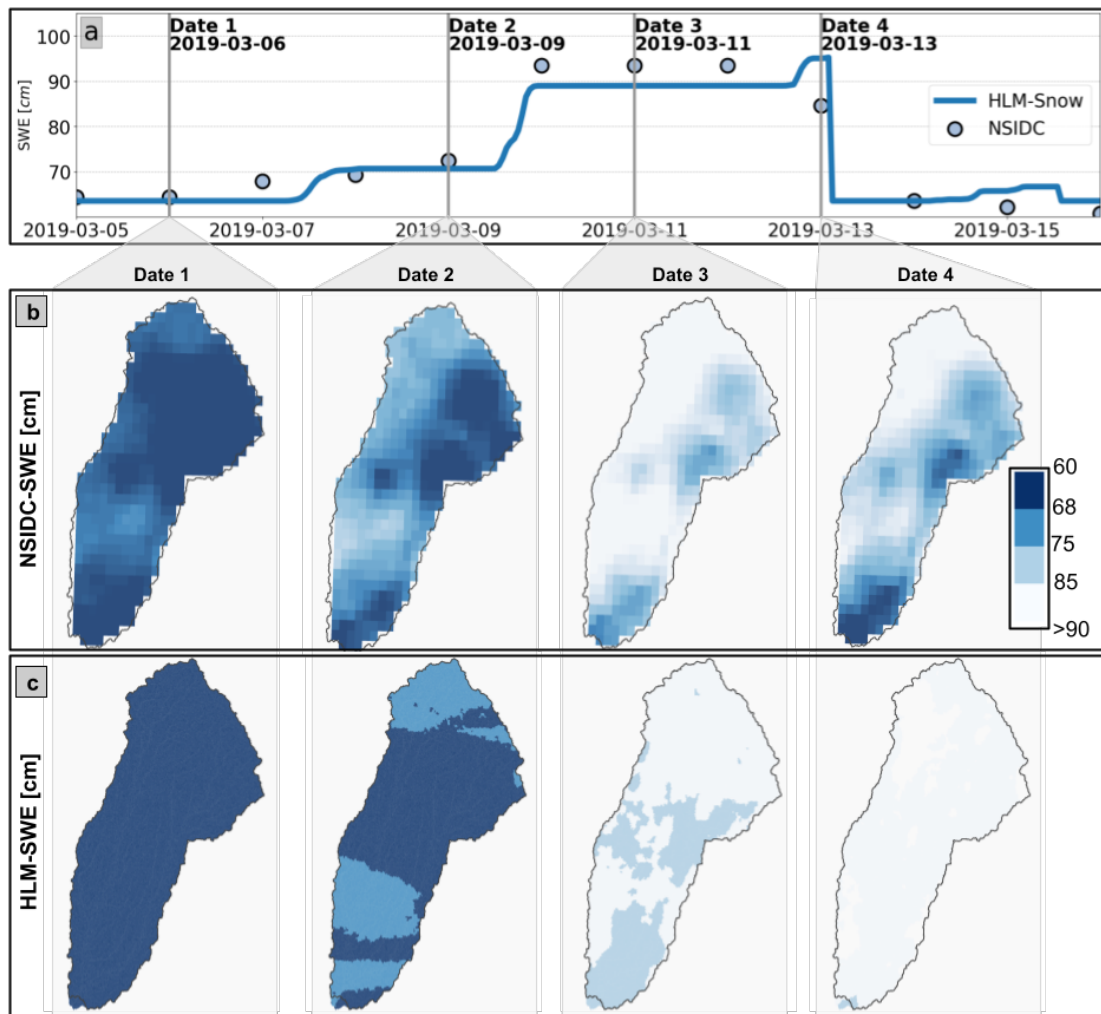


Figure 2.6 Mean SWE accumulation (in cm) during the March 2019 flood event. a) HLM (blue line) and NSIDC (dots) mean SWE over the Nishnabotna watershed. b) NSIDC SWE estimations for March 6, 9, 11, and 13. c) HLM-FSnow SWE estimations for March 6, 9, 11, and 13.

Furthermore, we tested HLM with the snow configuration for the state of Iowa between 2002 and 2020 using Stage IV rainfall and NARR temperature records. Figure 2.7 presents the KGE performance index for each USGS gauge in the state. KGE values oscillate between $-\infty$ and 1 (perfect simulation), and values above 0.2 are acceptable (Knoben et al., 2019). According to the model, it has a KGE of around 0.6 for the period. This value decreases to about 0.4 during the winter-to-spring transition period. Despite the decrease, the performance is still acceptable.

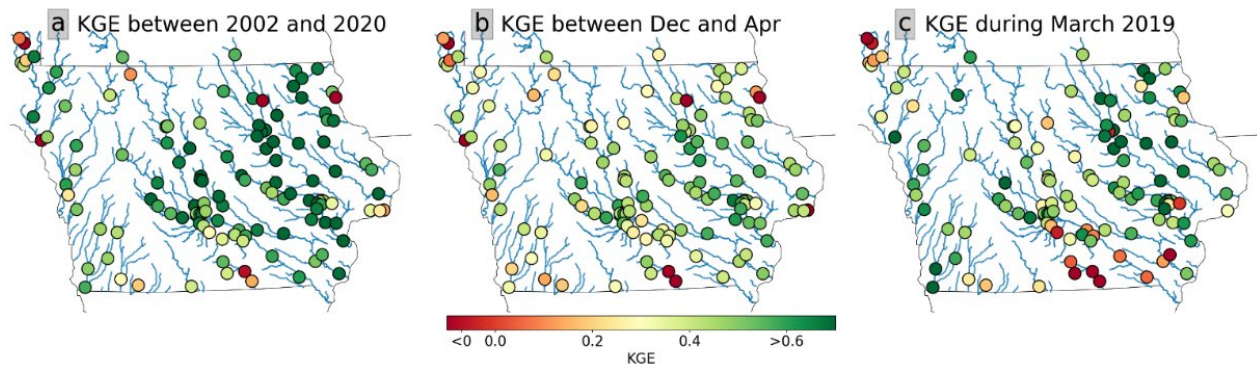


Figure 2.7 Mean KGE computed at the USGS gauges in Iowa using HLM-Snow. a) Long-term KGE comparing the observed records between 2002 and 2020. b) Mean KGE comparing only the results between December and April. c) March 2019 KGE.

Figure 2.8a and c present the ΔQ_p and KGE obtained during March 2019 versus the ratio of the observed peak flows ($q_{\max,2019}/q_{\max}$). According to the results, the ΔQ_p and the KGE improve with the event's magnitude. A similar result is observed in the spatial distribution of ΔQ_p (Figure 2.8b), where most of the gauges with an accurate peak flow estimation are over the West and center of Iowa. Moreover, around 60% of the gauges have a ΔQ_p value below 50% (Figure 2.8d).

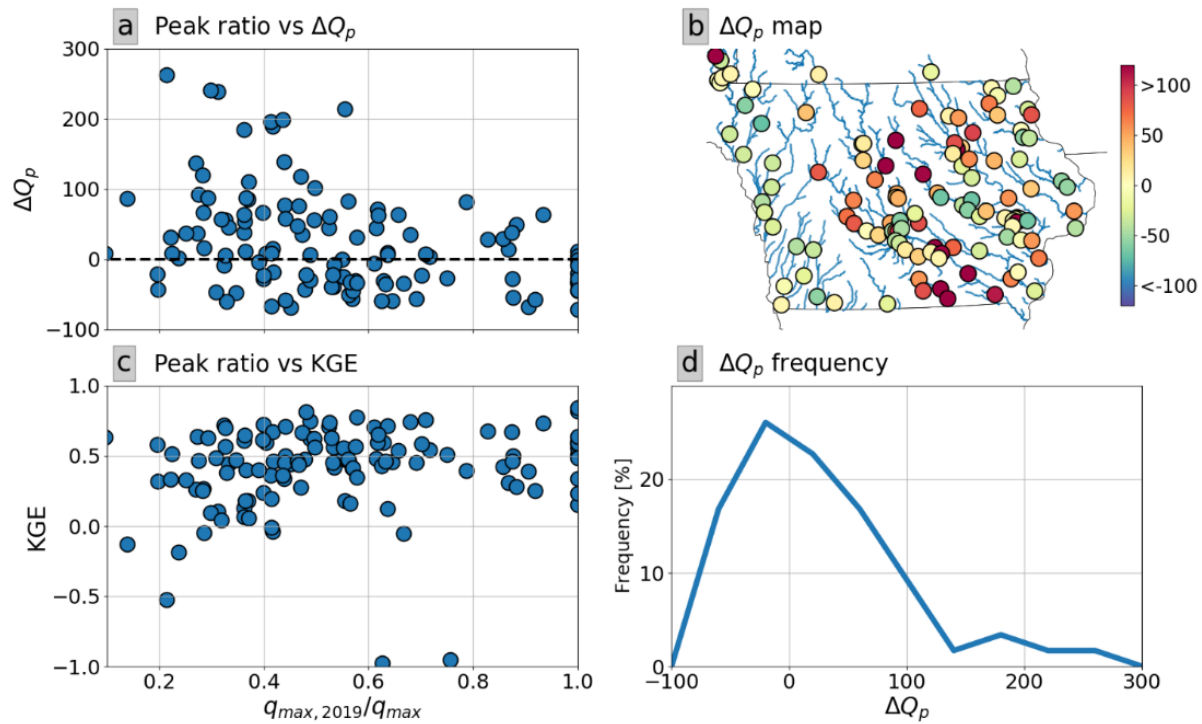


Figure 2.8 March 2019 event ΔQ_p and KGE performance in function of its observed magnitude or peak ratio ($q_{(\max,2019)}/q_{\max}$). a) peak ratio vs ΔQ_p , b) ΔQ_p estimated at each gauge, c) peak ratio vs. the KGE, and d) ΔQ_p frequency.

The results suggest that HLM-Snow can represent snow-related peak flows during the winter-to-spring transition. According to the KGE and ΔQ_p the model captures a significant portion of the observed oscillations and the large peaks. However, the model had limitations when representing low flows at this time of the year. Rainfall uncertainty and the snow model simplicity could be the leading causes of these limitations. Future work could expand on the development of the model and the variable involved in its performance during this transition period, as well as doing more in-depth research on different snow parameterizations and use of other rainfall products.

Currently, IFC is working on the operational implementation of the snow parameterization model for the state. Moreover, a complete description of the snow processes formulation and performance evaluation can be found in Velásquez et al. (2023).

2.3 Implementation of the TETIS model in HLM

We configured the TETIS model (Francés et al. 2007; Vélez, 2001) in HLM. In contrast with the Toplayer approach (Krajewski et al. 2017; Quintero et al. 2020), the TETIS model represents runoff processes using five storages. Figure 2.9 shows a schematic of the TETIS processes. The model uses six tanks to represent water storage in an extended soil column and the river. The tanks are called snow, static, surface, gravitational, aquifer, and channel. The vertical connections between tanks are the precipitation fluxes, snowmelt, evapotranspiration, infiltration, and percolation. The horizontal outputs from the tanks represent the overland flow, interflow, base flow, and total discharge.

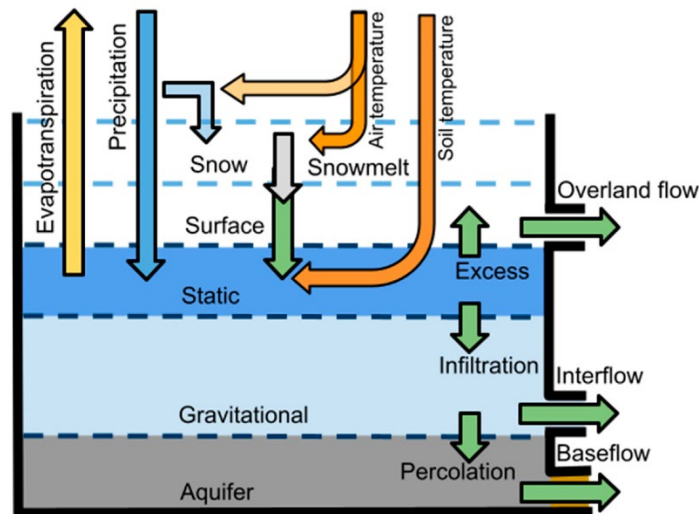


Figure 2.9 Schematic of the TETIS model structure in HLM.

We compared the model with the Toplayer using the described validation tool. Our results suggest that the TETIS approach can significantly improve specific regions of Iowa (see Figure 2.10).

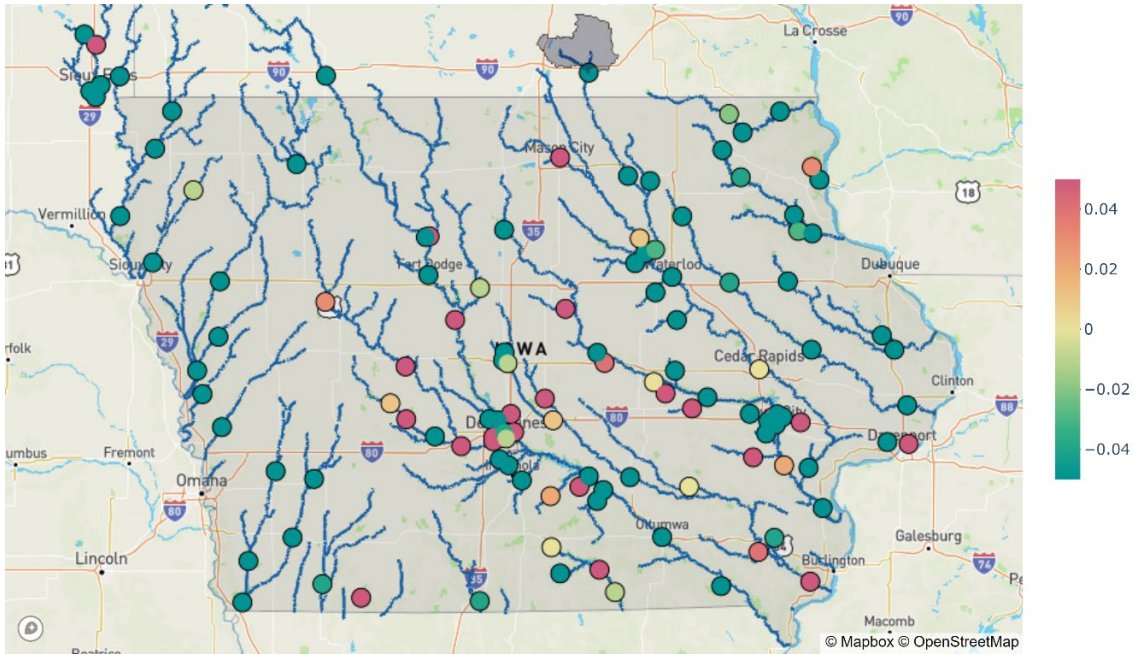


Figure 2.10 Difference between the TETIS KGE and Toplayer KGE. Positive values (red) represent regions where TETIS outperformed the Toplayer. Negative values (green) represent the opposite.

Figure 2.11 presents streamflow simulations at Des Moines Lobe and Western Iowa basins. In this area, previous model developments had challenges reproducing the hydrologic response (Quintero et al. 2020). The upper left panel shows the results for the Des Moines River basin at Fort Dodge, located in the Des Moines Lobe. Simulations from previous model structures (in purple) in this basin could not represent the discharge volumes in May and June as they did not account for snow melting, poorly replicated fallen limbs, and the hydrographs were recessed. With the new model structure (in green), an improvement is made in representing the

falling limbs and the recession during the last part of the year. Some issues in the rainfall input prevented a better volume estimation in May and during one event in December.

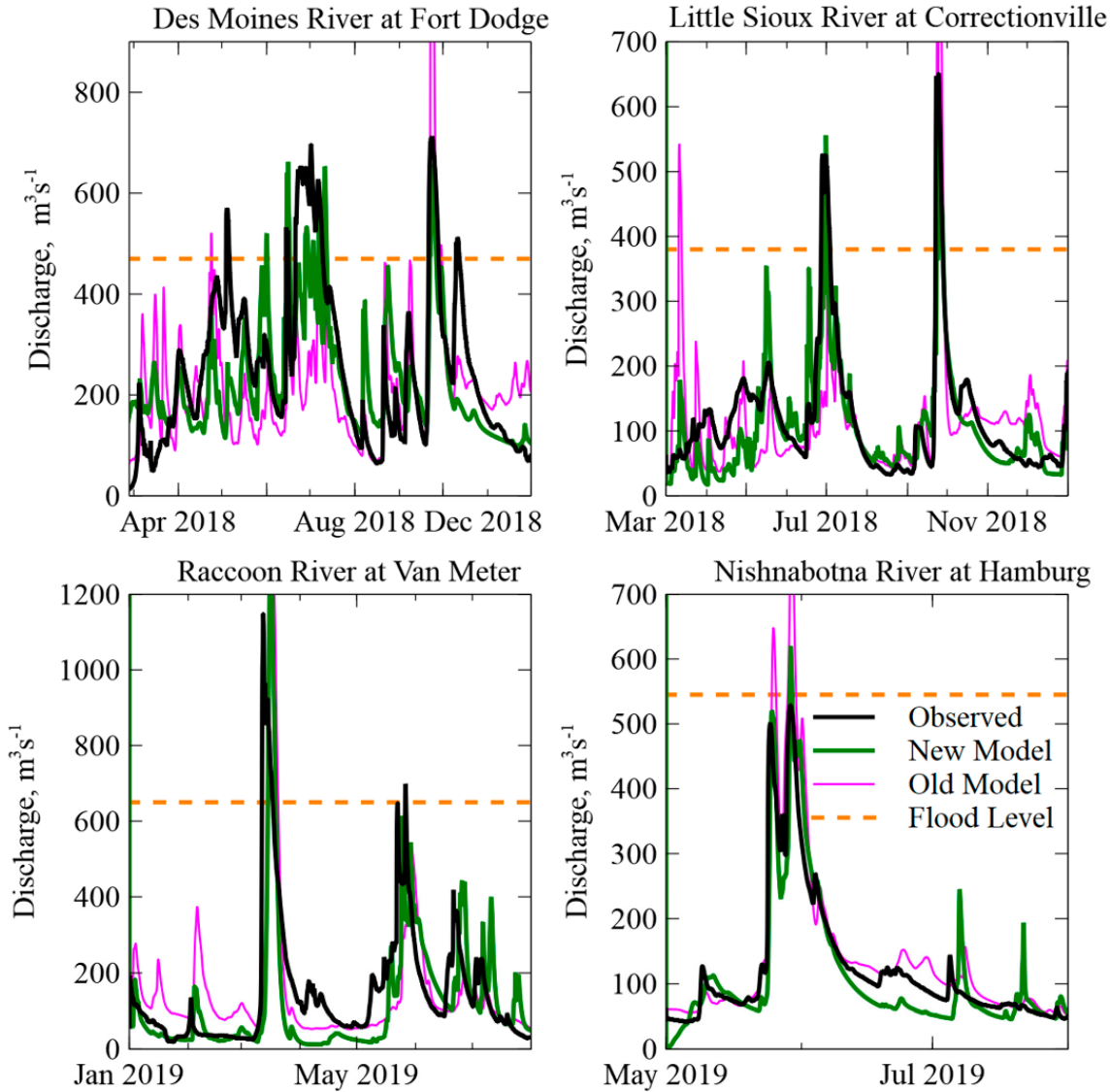


Figure 2.11 Flow simulations obtained at basins of the Des Moines Lobe landform (left column) and basins in Western Iowa.

A full description of the TETIS implementation can be found in Quintero, et al (2022).

2.4 Rainfall products evaluation

In tandem with the snow parameterization validation, we worked on testing a new rainfall product developed by the Iowa Flood Center (IFC). During the last years, IFC has provided rainfall estimates using the reflectivity (Z) value of the radars (IFC-RZ) (Krajewski et al. 2013; Seo et al. 2011, 2015; Seo and Krajewski, 2015). However, Z conversions tend to underestimate rainfall. Therefore, IFC developed a methodology to test the use of the specific attenuation measurement of the radar beam (IFC-RA). We ran HLM using both products (IFC-RA and IFC-RZ) between 2013 and 2019. Figure 2.12 presents the KGE performance index for each case over the state and their frequency distribution. According to our results, IFC-RA provided results comparable to MRMS, obtaining higher frequencies of KGE values above 0.6.

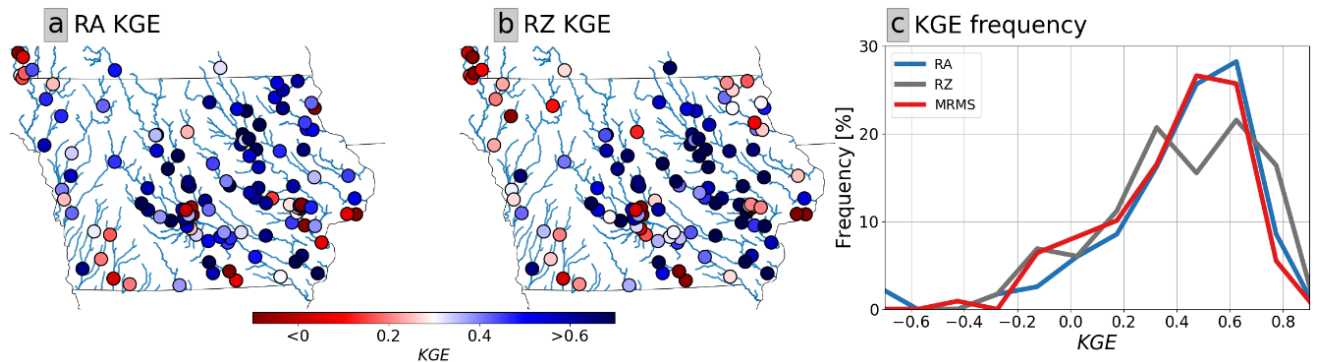


Figure 2.12 HLM KGE performance using IFC-RA (a) and IFC-RZ (b). The dots correspond to the USGS gauges in Iowa. c) presents the frequency distribution of both setups.

Additionally, we used the volumetric difference obtained by the model when using both products (Pbias). According to Figure 2.13, HLM using IFC-RA has lower volumetric bias than the versions using IFC-RZ and MRMS. Nevertheless, IFC-RA results exhibit overestimations in the southeast region of the state.

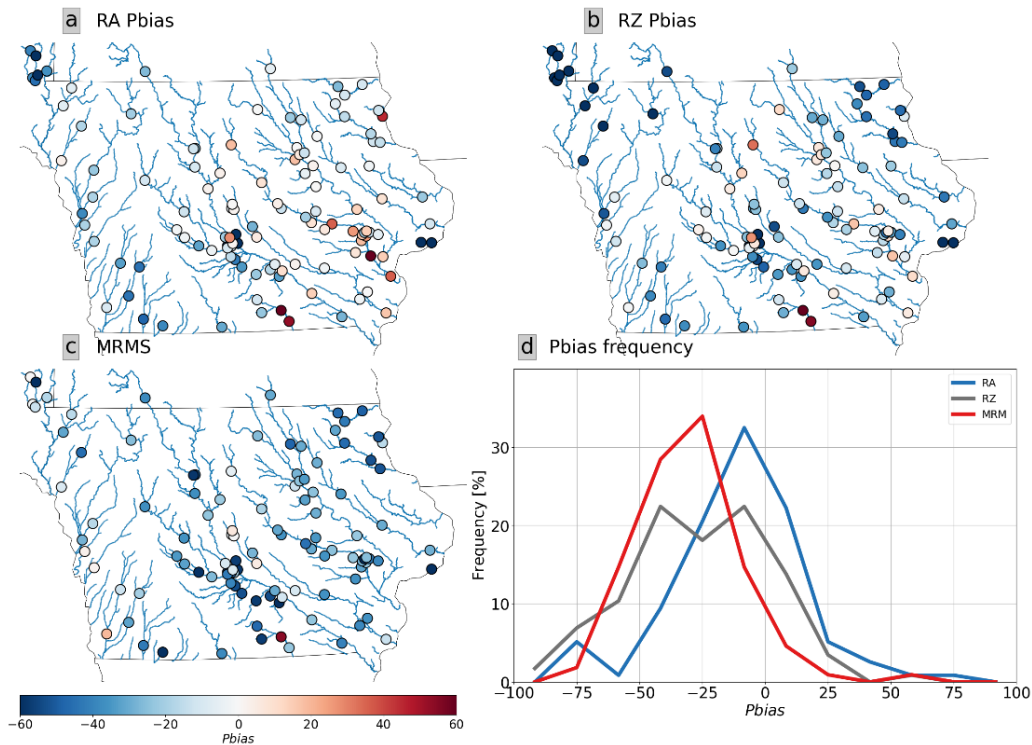


Figure 2.13 HLM volumetric bias using IFC-RA (a) and IFC-RZ (b) and MRMS (c). The dots correspond to the USGS gauges in Iowa. d) presents the frequency distribution of the three setups.

2.5 Upstream data assimilation

During Phase V, we developed a strategy to perform data assimilation (DA) upstream of a gauged reach. The DA uses streamflow data to estimate the routing parameters ν_0 and λ_1 (Mantilla, 2007). We created a hypothetical scenario to test the algorithm where the routing parameters randomly change inside the Skunk River Watersheds (Iowa). Then, we obtained synthetic streamflow observations at the outlet running HLM for the hypothetical scenario. Finally, we used the Ensemble Kalman Inversion (EKI) approach to guess those parameters using only the synthetic streamflow. In Figure 2.14, we present the differences between the provided and estimated parameters (a), and the differences between the synthetic streamflows and those obtained after using the EKI approach.

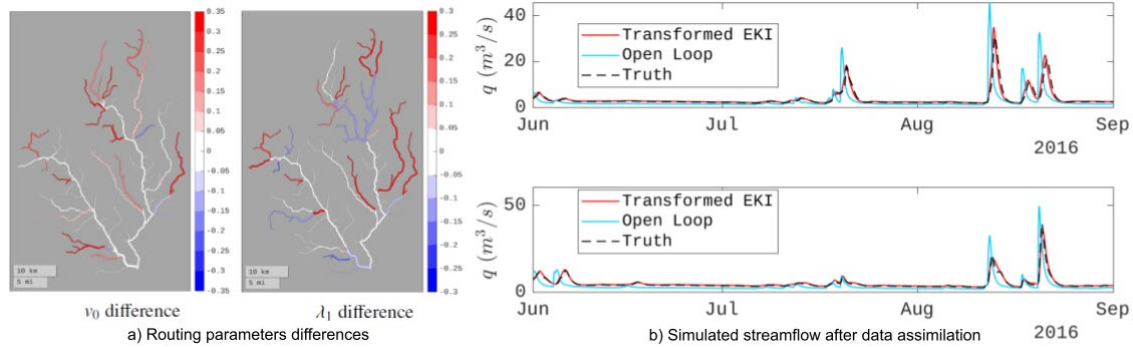


Figure 2.14 EKI Routing parameters estimation and simulated streamflow.

Furthermore, we also conducted experiments to improve HLM in a real-life scenario. We observed discharge records from twelve USGS gauges inside the Cedar River Watershed (Iowa) and used the Ensemble Kalman Filter Inversion (EKI) to assimilate downstream information to improve HLM simulations upstream. Using discharge records at the outlet, EKI generates a set of particles that change the model routing parameters. We evaluate the particles upstream, obtaining an envelope of possible model results at each link. Finally, we validated the EKI performance by comparing it with the upstream discharge observations. Figure 2.15 presents the results obtained at Shell Rock River. According to it, the mean behavior of the particles achieves a good representation of the observations improving the MRMS model reference run.

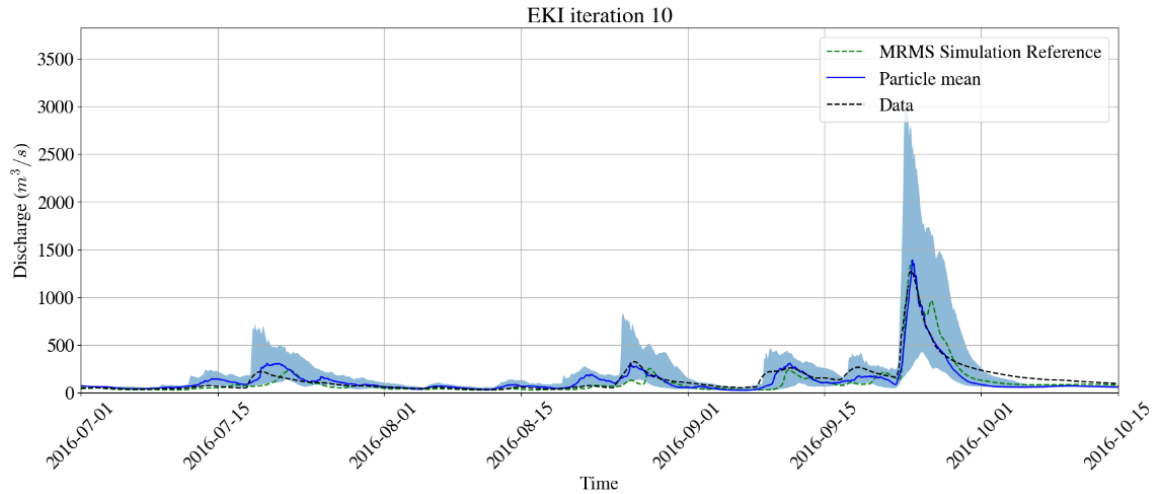


Figure 2.15 Results from the EKI data assimilation performed at Shell Rock River (4,487 km²) upstream of Cedar River (16,861 km²). The blue area represents the 10-90 interquartile region obtained by the particles, and the blue line is the particles' mean. The dashed black line represents the observed discharge, and the green line is the reference provided by HLM using MRMS without data assimilation.

Our EKI data assimilation results are promising as it provided accurate discharge forecasts. In the described approach, we used discharge observations to improve the forecast upstream. However, our results are limited to one flooding event in the Cedar River watershed. Further development will include exploring EKI implementation in other watersheds and for different rainfall events.

Chapter 3 Performance evaluation tool

We further explored HydroVise to develop a tool that allows us to validate our results (Jadidoleslam et al. 2020). We built our validation tool using Dash (<https://plotly.com/dash/>) for Python and Mapbox (<https://www.mapbox.com/>). We designed it to help us identify the strengths and shortcomings of our models' results and allow us to perform comparisons between parameterizations. The platform loads two top panels (see Figure 3.1).

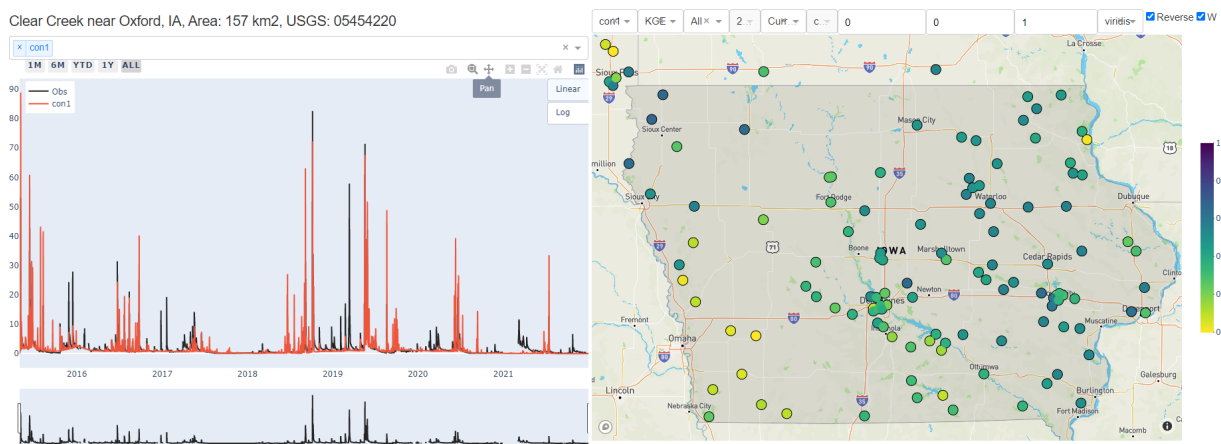


Figure 3.1 Top panels of the hydrologic modeling validation tool.

The left panel presents the observed streamflow records in the selected USGS gauge and is able to overlay results from multiple parameterizations, change the Y-axis scale, and navigate through the history of the results. For example, in Figure 3.2, we present the results from the simulation of three different HLM parameterizations at Clear Creek (USGS: 05454220). The panel includes information from the gauge, such as its name and total upstream area. It allows the selected parameterizations to turn off and on and move through the records.

Clear Creek near Oxford, IA, Area: 157 km2, USGS: 05454220

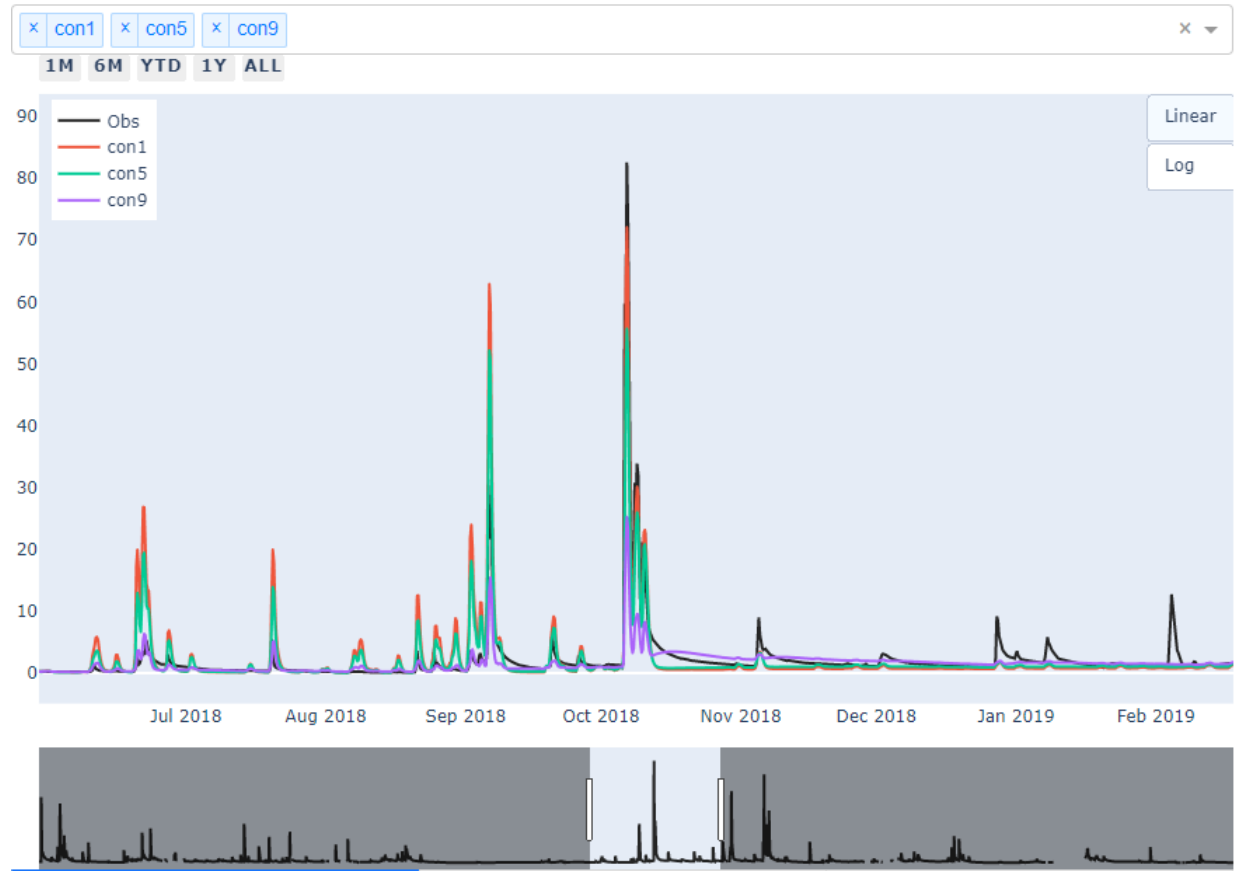


Figure 3.2 Streamflow plot panel showing the results for Clear Creek, Iowa.

The Y-axis is able to switch between linear and log scales. The linear scale is ideal for comparing peak flows, while the log scale is more suited for recessions and baseflow comparisons. Figure 3.3 presents an example of Figure 3.2 results in the log-scale.

Clear Creek near Oxford, IA, Area: 157 km², USGS: 05454220

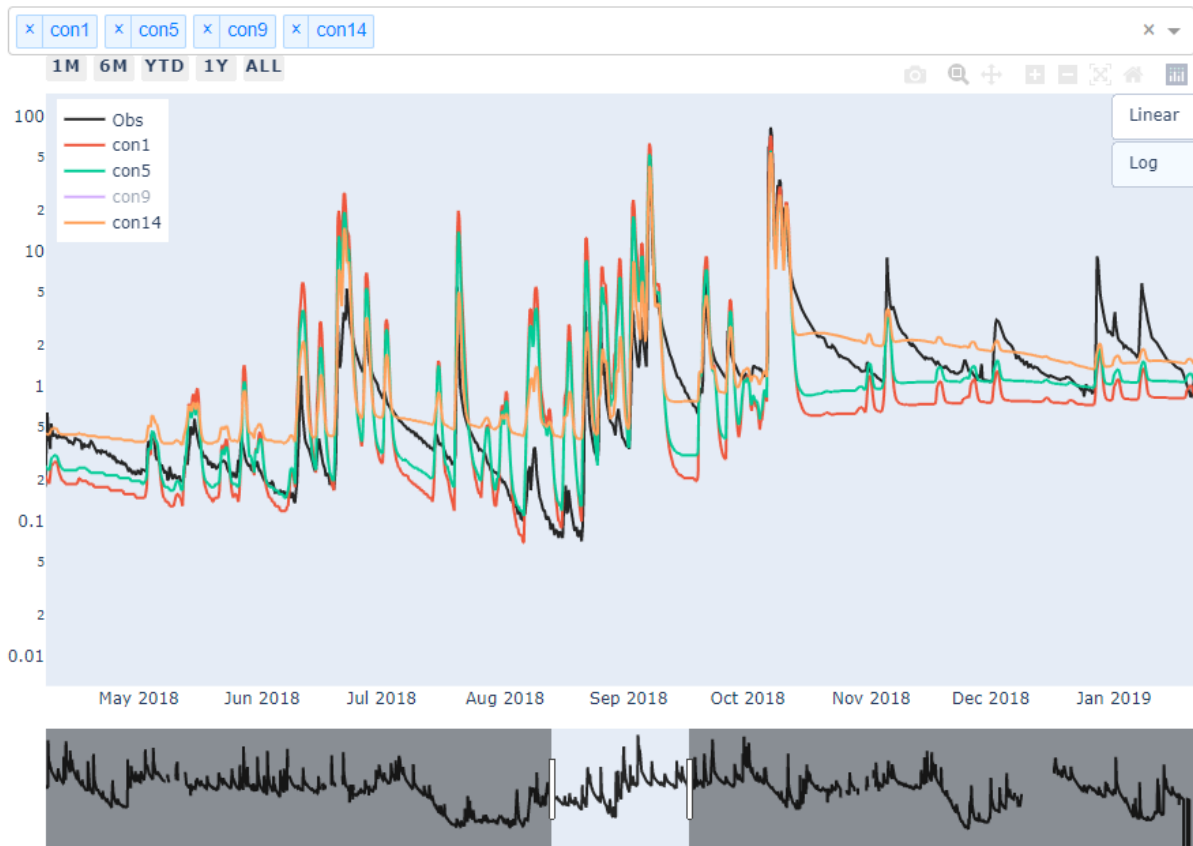


Figure 3.3 Streamflow plot panel showing the Clear Creek, Iowa results, in log-scale.

The right panel identifies spatial patterns of the model results. We included a list of several performance indexes, such as KGE and Nash. We also included options to change the color table and its range, as well as presenting the best parameterization by gauge or comparing two parameterizations using a selected performance index.

By adding the option to analyze simulation results by events, the user can select any specific event to analyze the detailed simulated and observed hydrographs and performance (see Figure 3.4).

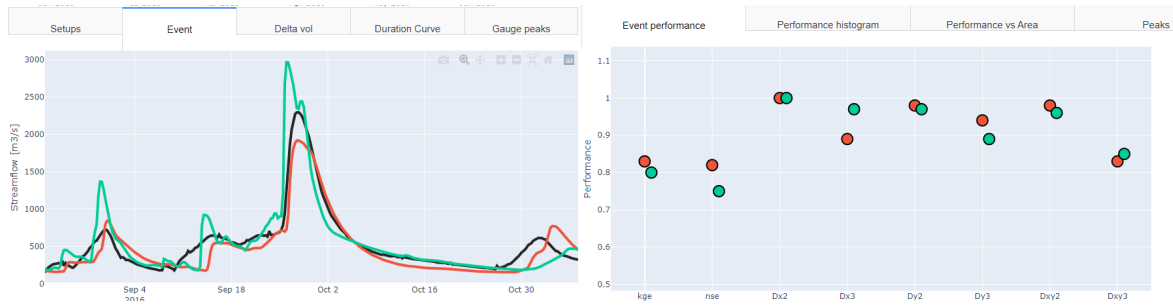


Figure 3.4 Event-based analysis using the platform.

We developed the validation software as a tool for implementing hydrological models at a regional level. It is an ongoing work that has helped us identify the main shortcomings of HLM in Iowa. However, its application can be expanded to other areas and include additional hydrological models. Future developments will include panels to present the performance parameters' distributions and compare simulated and observed peak flows.

Chapter 4 Technology transfer

We successfully transferred our HLM knowledge to the researchers at the University of Nebraska during the last months of this phase. The transfer included the implementation of HLM-Snow in their server and the installation of eight bridge sensors over the Elkhorn River network.

4.1 HLM implementation

The transfer started by implementing a snow model that mimics the accumulation and melting of snow during the early spring season. Figure 4.1 presents the average Snow Water Equivalent (SWE) observed (blue) and simulated (orange) for the area of the Elkhorn River in Nebraska. Despite the model's simplicity, it successfully represents the observed SWE oscillations in the region.

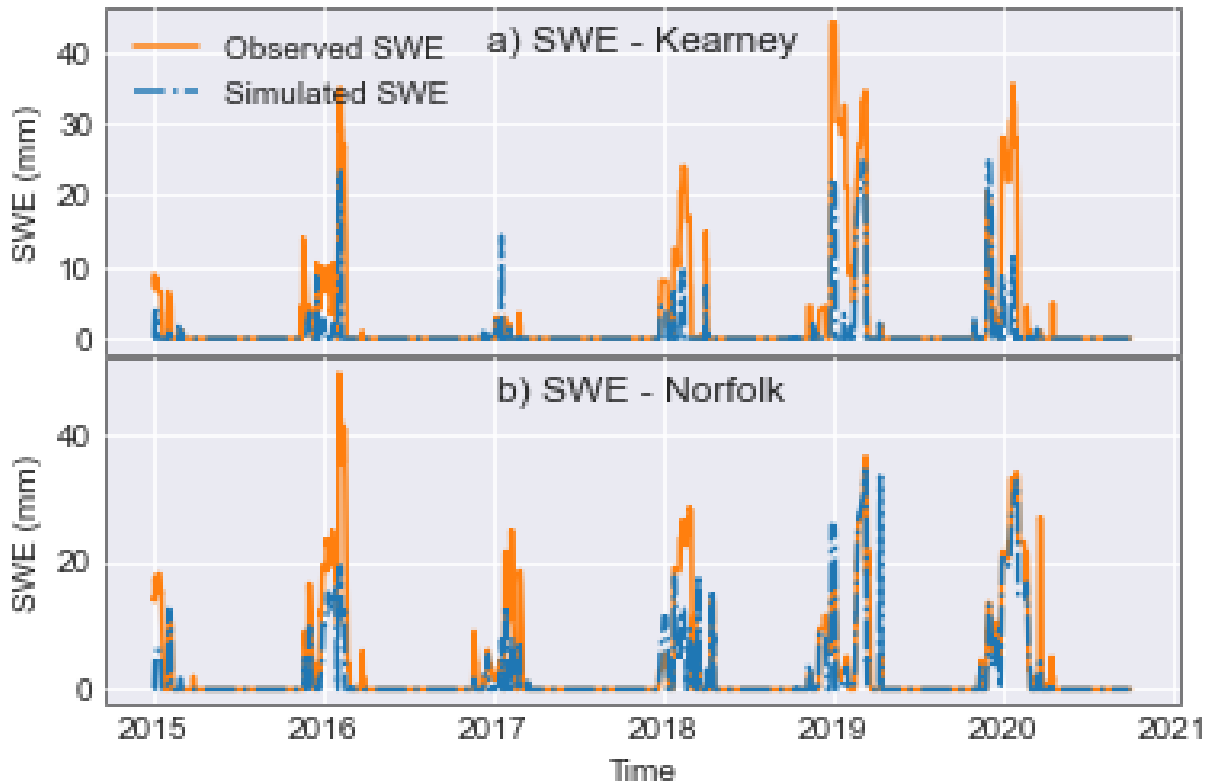


Figure 4.1 Mean Observed (orange) and simulated (blue) SWE over the Elkhorn watershed.

After testing the SWE model, we transferred HLM and implemented it on the Elkhorn River Watershed. We used temperature records from NLDAS and stage-IV rainfall estimations in the implementation. Figure 4.2 presents the snow water equivalent (SWE) simulated by HLM in the Elkhorn watershed. According to it, the HLM-Snow parameterization can reproduce most of the observed discharge oscillations due to snowmelt.

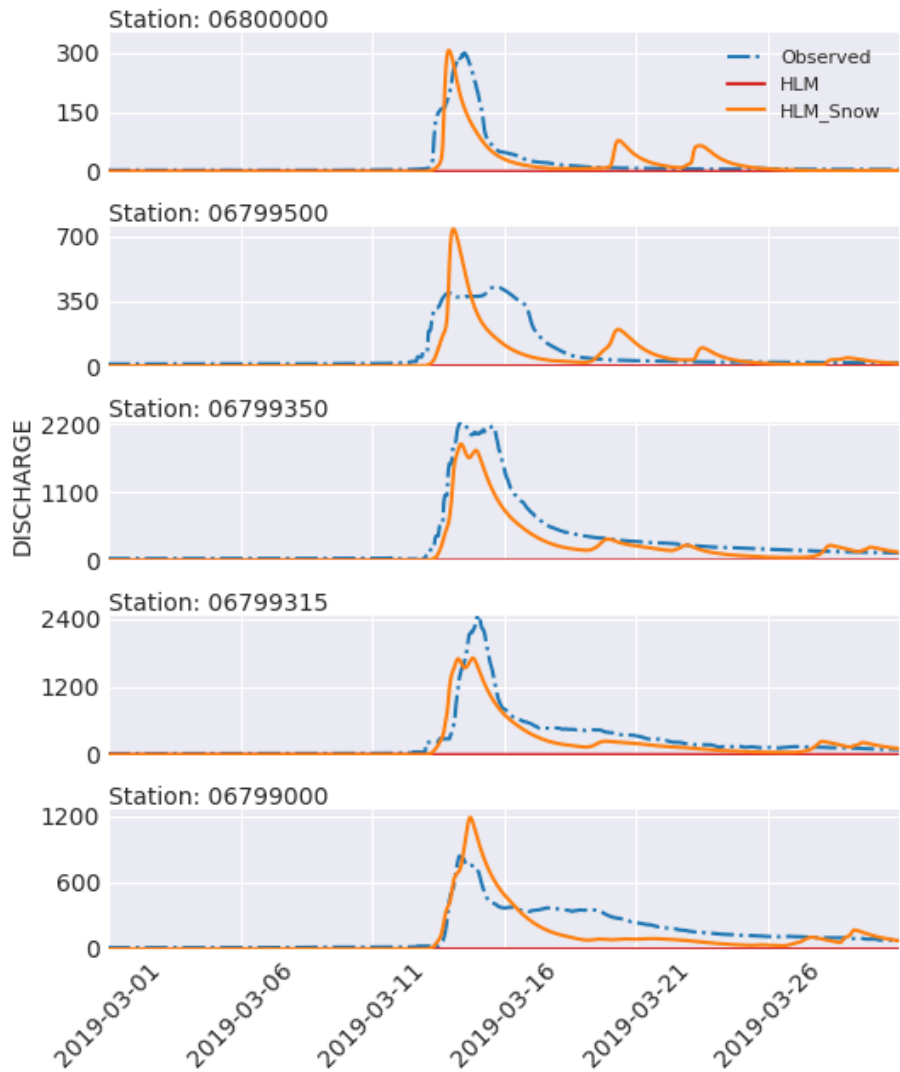


Figure 4.2 HLM-Snow simulations at the Elkhorn River Watershed for March 2019.

Along with the model development and implementation, we helped the University of Nebraska build a web platform to display the hydrological simulation results. Figure 4.3 presents a snapshot of the platform implemented for the Elkhorn River Watershed. Like the platform described in Chapter 3, their implementation has a map of the watershed and its network. It also

has a panel to present the observations and the model results and a panel to present the properties of the selected USGS gauge.

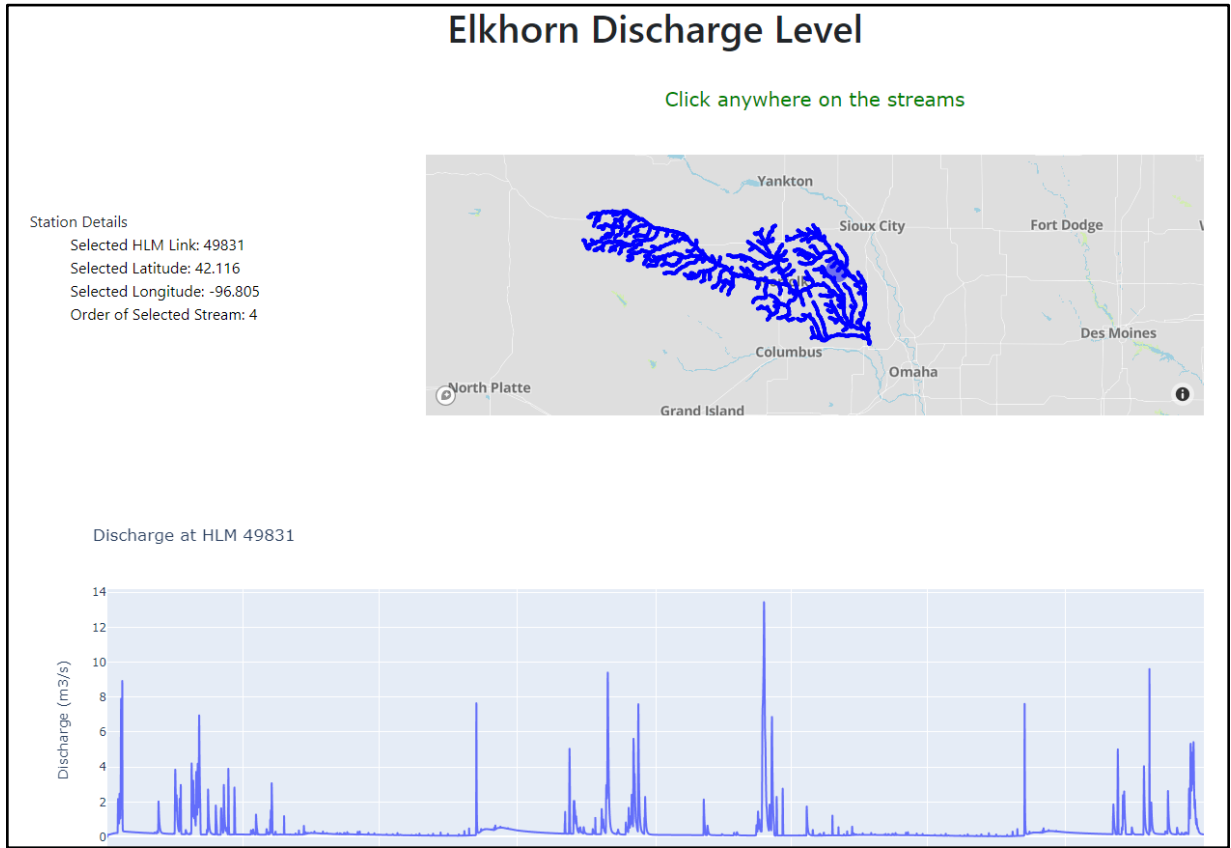


Figure 4.3 Elkhorn River web platform example.

4.2 Bridge sensors installation

We installed eight sensors over the Elkhorn River, Nebraska, reporting level observations every 15 minutes. The sensors emit a sonar signal toward the stream to measure the distance between the sensor and the water table. First, we determined the localization of the sensors to cover tributaries not observed by the USGS network. Then, we refined the localization based on the field conditions. Figure 4.4 shows the Elkhorn network, the USGS, and the newly installed sensors.

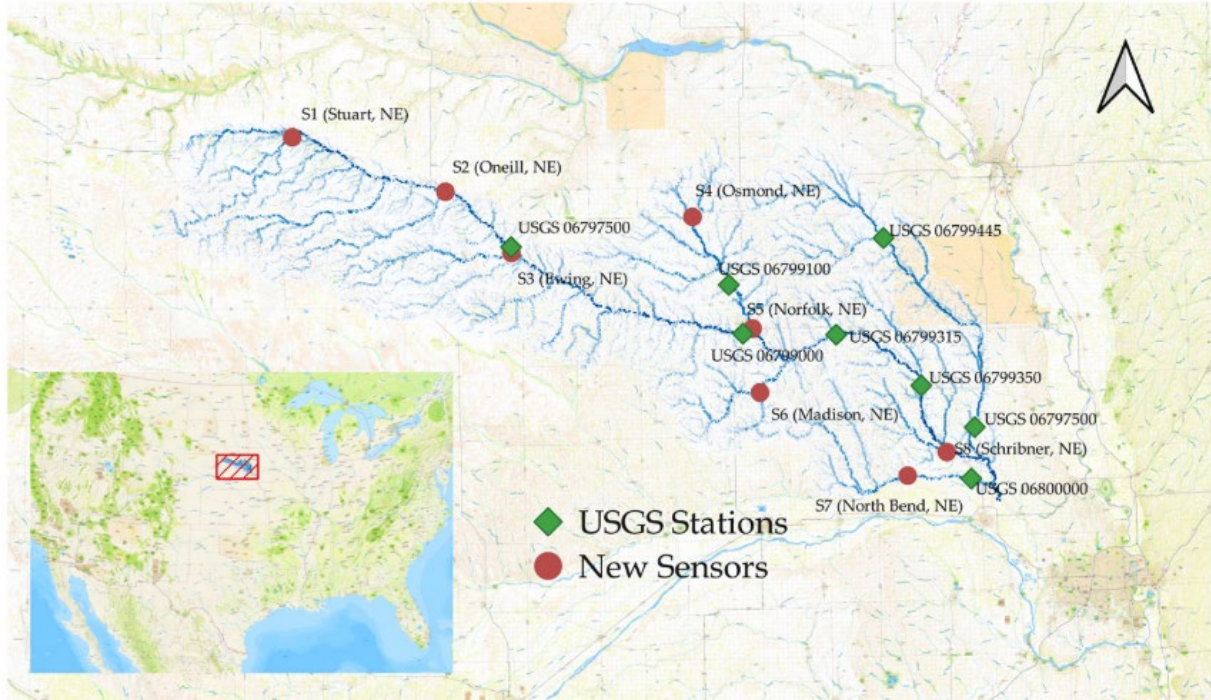


Figure 4.4 Elkhorn River Network (blue lines), USGS gauges (green), and installed bridge sensors (red). Image taken from Koya et al. (2023).

The bridge sensors report water level; however, we require discharge to validate the hydrological model. Therefore, we converted the level to discharge using rating curves. We built synthetic rating curves using the HEC-RAS hydraulic model. We set up the model using the section bathymetry at each gauge and obtained discharge observations for different level values. Figure 4.5 presents the synthetic rating curves obtained for each sensor.

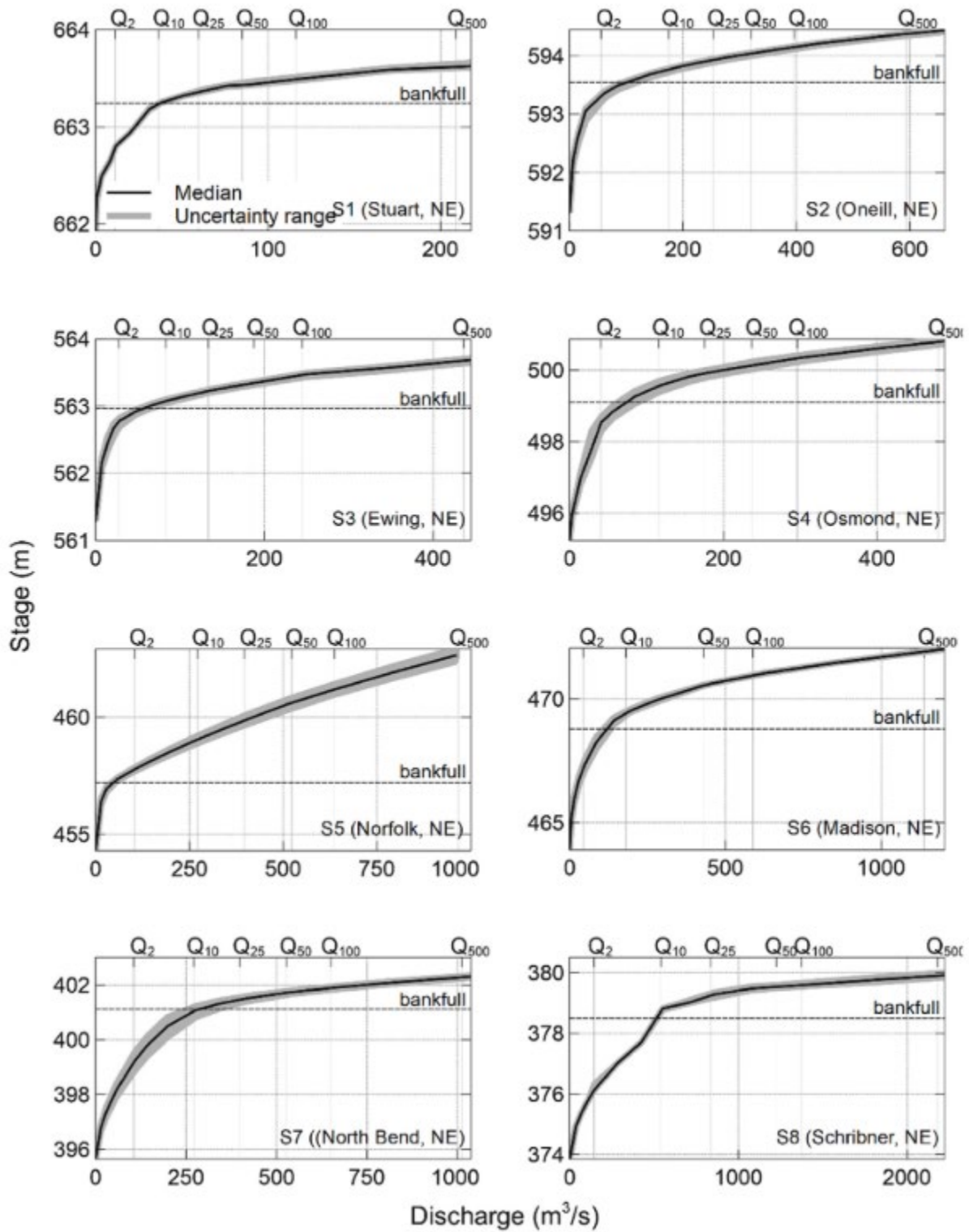


Figure 4.5 Synthetic rating curves developed for each installed level gauge. Taken from Koya et al. (2023).

Currently, the sensors report observations to IFIS. Nevertheless, the University of Nebraska accesses it through an FTP service. A full description and the results derived from the described collaboration can be found in Koya et al. (2021).

Chapter 5 Conclusions

An essential aspect of providing a safe, efficient, and effective transportation system is anticipating natural hazards that can lead to road closures. Extreme floods can lead to bridge overtopping and/or compromising the structural integrity of river overpasses, including box culverts. The flood forecasting model and information system proposed here provides a tool to anticipate potential hazardous flood-related situations. It would allow time to initiate action plans to minimize the impact on the overall transportation system. The forecasting model can be used in real-time to anticipate floods and to look at past flooding scenarios to determine if all actions taken were appropriate or can be improved. Our forecasting system will improve safety and minimize the risk of increasing multi-modal freight movements on the U.S. surface transportation system by enhancing safety and warning of potential road closures.

As part of this project, we have provided a prototype forecasting platform with five specific innovations. 1) A high-definition network that identifies better bridge intersections and areas of interest, 2) The incorporation of snow processes to simulate early spring floods, 3) The implementation of the TETIS scheme to simulate runoff processes, 4) The development of a data assimilation method that improves forecasts using downstream observations, and 5) the development of a platform that compares model configurations at the state level. Our developments give us confidence that we can continue developing a forecasting system that is transferable to other locations in the Midwest. As floods continue to be the costliest disaster in the nation, it becomes critical that tools are developed to better predict them.

Bibliography

- Ayalew, T. B., Krajewski, W. F., & Mantilla, R. (2014). Connecting the power-law scaling structure of peak-discharges to spatially variable rainfall and catchment physical properties. *Advances in Water Resources*, *71*, 32–43. <https://doi.org/10.1016/j.advwatres.2014.05.009>
- Cunha, L. K., Mandapaka, P. V., Krajewski, W. F., Mantilla, R., & Bradley, A. a. (2012). Impact of radar-rainfall error structure on estimated flood magnitude across scales: An investigation based on a parsimonious distributed hydrological model. *Water Resources Research*, *48*(10), n/a-n/a. <https://doi.org/10.1029/2012WR012138>
- Felipe Quintero, N. V. (2022). Implementation of TETIS Hydrologic Model into the Hillslope Link Model Framework. *Water*, *14*(17), 2610.
- Francés, F., Vélez, J. I., & Vélez, J. J. (2007). Split-parameter structure for the automatic calibration of distributed hydrological models. *Journal of Hydrology*, *332*(1–2), 226–240. <https://doi.org/10.1016/j.jhydrol.2006.06.032>
- Gupta, V. K., & Waymire, E. C. (1998). Spatial Variability and Scale Invariance in Hydrologic Regionalization. In G. Sposito (Ed.), *Scale Dependence and Scale Invariance in Hydrology* (pp. 88–135). Cambridge University Press. <https://doi.org/10.1017/CBO9780511551864.005>
- Jadidoleslam, N., Goska, R., Mantilla, R., & Krajewski, W. F. (2020). Hydrovise: A non-proprietary open-source software for hydrologic model and data visualization and evaluation. *Environmental Modelling and Software*, *134*, 104853. <https://doi.org/10.1016/j.envsoft.2020.104853>
- Kienzle, S. (2008). A new temperature based method to separate rain and snow. *Hydrological Processes*, *22* (November 2008), 5067–5085. <https://doi.org/10.1002/hyp>
- Knoben, W. J. M., Freer, J. E., & Woods, R. A. (2019). Technical note: Inherent benchmark or not? Comparing Nash-Sutcliffe and Kling-Gupta efficiency scores. *Hydrology and Earth System Sciences*, *23*(10), 4323–4331. <https://doi.org/10.5194/hess-23-4323-2019>
- Koya, S. R., Velasquez, N., Mantilla, R. I., Rojas, M., Harvey, K., Ceynar, D., Krajewski, W. F., & Roy, T. (2023). A Prototype Flood Forecasting System for Nebraska Watersheds. *Environmental Modelling and Software*, *164* (April), 105693. <https://doi.org/10.1016/j.envsoft.2023.105693>
- Krajewski, Witold F., Kruger, A., Singh, S., Seo, B. C., & Smith, J. A. (2013). Hydro-NEXRAD-2: Real-time access to customized radar-rainfall for hydrologic applications. *Journal of Hydroinformatics*, *15*(2), 580–590. <https://doi.org/10.2166/hydro.2012.227>
- Krajewski, Witold F., Ceynar, D., Demir, I., Goska, R., Kruger, A., Langel, C., Mantilllla, R., Niemeier, J., Quintero, F., Seo, B. C., Smallll, S. J., Weber, L. J., & Young, N. C. (2017). Real-time flood forecasting and information system for the state of Iowa. *Bulletin of the*

- American Meteorological Society*, 98(3), 539–554. <https://doi.org/10.1175/BAMS-D-15-00243.1>
- Mantilla, R., & Gupta, V. K. (2005). A GIS numerical framework to study the process basis of scaling statistics in river networks. *IEEE Geoscience and Remote Sensing Letters*, 2(4), 404–408. <https://doi.org/10.1109/LGRS.2005.853571>
- Mantilla, Ricardo (2007). Physical Basis of Statistical Scaling in Peak Flows and Stream Flow Hydrographs for Topologic and Spatially Embedded Random Self-similar Channel Networks. *Analysis*.
- Quintero, F., Krajewski, W. F., Seo, B. C., & Mantilla, R. (2020). Improvement and evaluation of the Iowa Flood Center Hillslope Link Model (HLM) by calibration-free approach. *Journal of Hydrology*, 584(February), 124686. <https://doi.org/10.1016/j.jhydrol.2020.124686>
- Koya, S., Velasquez, N., Mantilla, R., Rojas, M., Harvey, K., Ceynar, D., Krajewski, W., & Roy, T. (2021). Development of a Flood Monitoring System Prototype for a Pilot Basin in Nebraska. *AGU Fall Meeting Abstracts, 2021*, C35G–0966.
- Seo, B. C., & Krajewski, W. F. (2015). Correcting temporal sampling error in radar-rainfall: Effect of advection parameters and rain storm characteristics on the correction accuracy. *Journal of Hydrology*, 531, 272–283. <https://doi.org/10.1016/j.jhydrol.2015.04.018>
- Seo, B. C., Krajewski, W. F., Kruger, A., Domaszczynski, P., Smith, J. A., & Steiner, M. (2011). Radar-rainfall estimation algorithms of Hydro-NEXRAD. *Journal of Hydroinformatics*, 13(2), 277–291. <https://doi.org/10.2166/hydro.2010.003>
- Seo, B. C., Krajewski, W. F., & Mishra, K. V. (2015). Using the new dual-polarimetric capability of WSR-88D to eliminate anomalous propagation and wind turbine effects in radar-rainfall. *Atmospheric Research*, 153, 296–309. <https://doi.org/10.1016/j.atmosres.2014.09.004>
- Velásquez, N., Quintero, F., Koya, S. R., Roy, T., & Mantilla, R. (2023). Snow-detonated floods: Assessment of the U.S. midwest march 2019 event. *Journal of Hydrology: Regional Studies*, 47. <https://doi.org/10.1016/j.ejrh.2023.101387>
- Vélez, J. I. (2001). Desarrollo de un modelo hidrológico conceptual y distribuido orientado a la simulación de crecidas. *Tesis Doctoral - Universidad Politécnica de Valencia*, 266.